Topolectrical Circuits

Ching Hua Lee[1,2], Stefan Imhof[3], Christian Berger[3], Florian Bayer[3], Johannes Brehm[3], Laurens W. Molenkamp[3], Tobias Kiessling[3] & Ronny Thomale [4]

Invented by Alessandro Volta and Félix Savary in the early 19th century, circuits consisting of resistor, inductor and capacitor (RLC) components are omnipresent in modern technology. The behavior of an RLC circuit is governed by its circuit Laplacian, which is analogous to the Hamiltonian describing the energetics of a physical system. Here we show that topological insulating and semimetallic states can be realized in a periodic RLC circuit. Topological boundary resonances (TBRs) appear in the impedance read-out of a topolectrical circuit, providing a robust signal for the presence of topological admittance bands. For experimental illustration, we build the Su-Schrieffer–Heeger circuit, where our impedance measurement detects the TBR midgap state. Topolectrical circuits establish a bridge between electrical engineering and topological states of matter, where the accessibility, scalability, and operability of electronics synergizes with the intricate boundary properties of topological phases.

[1] Institute of High Performance Computing, A*STAR, Singapore 138632, Singapore. [2] Department of Physics, National University of Singapore, Singapore 117542, Singapore. [3] Experimentelle Physik 3, Physikalisches Institut, University of Würzburg, Am Hubland, D-97074 Würzburg, Germany. [4] Institute for Theoretical Physics and Astrophysics, University of Würzburg, Am Hubland, D-97074 Würzburg, Germany. Correspondence and requests for materials should be addressed to R.T. (email: rthomale@physik.uni-wuerzburg.de)

Topological semimetals[1] constitute the latest development of an evolution dating back more than 30 years, when topological phases began to cast their shadows before as midgap states in polyacetylene[2] and the quantized edge modes of integer quantum Hall systems[3] were discovered. Driven by the flourishing field of topological insulators[4, 5], the viewpoint of topology has recently branched out to various classes of physical systems, ranging from electrons in solids to photonic networks in metamaterials, ultra-cold atoms in optical lattices, microwave resonators, electrical circuits, and phonons in mechanical setups (see e.g. refs.[6–13]). Note that such topological states of matter do not necessarily rely on any quantum mechanical framework. In mathematical terms, it is not the quantum, i.e., non-commutative, nature of the Hilbert space, but rather the nontrivial connectivity of phase space under cyclic evolution of parameters[14] that indicates a topological phase.

The fingerprint of a topological insulator motif, independent of the physical setting in which it is realized, is given by a single edge mode response protected by topology, along with an unresponsive bulk. Note that whereas time-reversal symmetry T, if preserved, may protect the quantum realization of a topological insulator against elastic backscattering due to $T^2 = -1$ for electrons[4, 5], there is no such additional robustness for classical realizations due to $T^2 = 1$ for its constituting degrees of freedom. While there are various promising approaches to realize a topological insulator within classical arrays, topological device design is often limited due to insufficient edge mode density. As opposed to fermionic systems where the chemical potential is a useful parameter to access any particular range of the band structure at low energies, bosonic or classical degrees of freedom for a topological band structure also pose the problem how to systematically address the spectral regime of interest, such as the band gap domain of a topological insulator. Furthermore, in an era where classical experimental setups for topological phases still need to improve in terms of uniformity of array elements, it is often challenging to resolve single edge mode responses to identify the onset of a topological insulator phase.

We propose the topological semimetal paradigm in classical RLC circuits, which predicts highly pronounced resonances in a generic impedance read-out whenever there are topological boundary modes that scale extensively, such as the Fermi arcs of topological semimetals[15]. Due to their extensive degeneracy, such topological boundary resonances (TBRs) remain robust even in the face of significant nonuniformity of circuit elements, promising high-precision identification in a realistic measurement. We outline a detailed design of such topolectrical circuits, including a Weyl circuit network exhibiting TBRs of Fermi arc type, where the AC driving frequency combined with the grounding design takes over the role of the chemical potential in a fermionic system. As an initial proof-of-principle experimental study, we report impedance and voltage profile measurements of the Su–Schrieffer–Heeger circuit chain. As a theoretical byproduct in this work, we further introduce the mathematical framework for characterizing topological properties of electrical circuit graphs in general. While our semimetal paradigm can be applied to any classical array setup such as mechanical systems or optical cavities, the topolectrical circuits we introduce combine all desired conceptual and experimental preferences to realize topological semimetal analogs in a classical model, without demanding specialized equipment.

Results

Laplacian formalism. Any electrical circuit network can be represented by a graph whose nodes and edges correspond to the circuit junctions and connecting wires/elements. The circuit
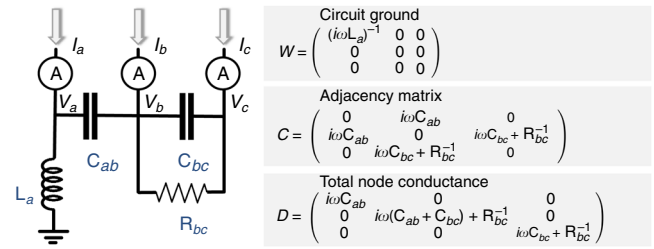

Fig. 1 Definition of the principal building blocks for the grounded circuit Laplacian $J = D - C + W$ (Eq. (2)) of an illustrative RLC circuit with nodes $\{a, b, c\}$. W and D are diagonal matrices containing the total conductances from each node towards the ground and towards the rest of the circuit, respectively. C is the adjacency matrix of the circuit graph, with edges weighted by their conductances

behavior is fundamentally described by Kirchhoff's law

$$I_a = \sum_i C_{ai}(V_a - V_i) + w_a V_a, \quad (1)$$

where I_a and V_a are the input current and electrical potential at each node a. By current conservation, I_a equals the total current flowing out of node a towards all other nodes i linked by nonzero conductance C_{ai}, plus the current flowing into the ground through a route with impedance w_a^{-1}. The impedance and conductances are real for resistive circuit elements, but will be complex when capacitors or inductors are present (Fig. 1). As an initial step towards identifying circuits with tight-binding lattice models, we rewrite Eq. (1) in compact matrix form

$$\mathbf{I} = (L + W)\mathbf{V} = J\mathbf{V}, \quad (2)$$

with vectors $\mathbf{V}$ and $\mathbf{I}$ formed by the components V_a and I_a. The grounded Laplacian J, as defined in Eq. (2), consists of L, the circuit Laplacian which depends on the conductance network structure, and $W = \text{diag}(w_1, w_2, \ldots)$, which depends on how the circuit is grounded. The Laplacian is defined in terms of the conductances by $L = D - C$, where C is the (adjacency) matrix of conductances and $D = \text{diag}(\sum_i C_{1i}, \sum_i C_{2i}, \ldots)$ lists the total conductances out of each node (Fig. 1). To understand the relation of L with the continuum Laplacian, one writes the spreading of current from a single node as a divergence of current density $I = \nabla \cdot \mathbf{j}$, and invokes the definition of conductivity $\mathbf{j} = \sigma \mathbf{E} = \sigma \nabla V$. Hence, for the current and voltage vectors as in Eq. (2), $\mathbf{I} = \nabla \cdot (\sigma \nabla)\mathbf{V} = L\mathbf{V}$. This establishes L as the continuum Laplacian restricted to a circuit.

A circuit is most commonly studied through an impedance measurement, which involves running a current through it and measuring the voltage response. As capacitive and inductive resistances explicitly depend on it, the driving voltage frequency ω is a central tuning parameter of topolectrical circuits. The simplest measurement is the two-point impedance $Z_{ab} = (V_a - V_b)/I$ between nodes a and b, where $V_a - V_b$ is their potential difference and I is the magnitude of the current $I_{a,b} = \pm I$ that enters at a and leaves at b. To determine Z_{ab}, the potentials have to be expressed in terms of the input current by inverting Eq. (2). For this purpose, we employ the regularized inverse of J known as the circuit Green's function $G = \sum_{j_n \neq 0} \frac{1}{j_n} \psi_n \psi_n^\dagger$, where j_n and ψ_n denote the admittance eigenvalues and the N-dimensional eigenmode vectors of J, respectively. (Regularization in this context means that $j_n = 0$ modes are omitted when the circuit is not grounded ($W = 0$) and hence defined up to an overall potential offset. If J is not Hermitian, $\psi_n^\dagger$ and ψ_n are replaced by the left and right eigenvectors.) The eigenmodes are potential distributions proportional to the input current distribution. Note

that G is always symmetric when the circuit elements are reciprocal (see also ref. [16]). The two-point impedance reads[17]

$$
\begin{aligned}
Z_{ab} &= \sum_{i=a,b} \frac{G_{ai}I_i - G_{bi}I_i}{I} = G_{aa} + G_{bb} - G_{ab} - G_{ba} \\
&= \sum_{j_n \neq 0} \frac{|\psi_{n,a} - \psi_{n,b}|^2}{j_n},
\end{aligned}
\tag{3}
$$

where $\psi_{n,a} - \psi_{n,b}$ is the difference between the amplitudes of the nth admittance eigenmode. As such, the impedance in Eq. (3) for each mode n depends on the squared magnitude of its potential difference between a and b, weighted by its eigen-impedance j_n^{-1}.

To make contact with topological band structures, we consider circuits made up of periodic sublattices. A node $a = (\mathbf{x}, s)$ can be indexed by its unit cell position $\mathbf{x}$ and sublattice label s. Due to translation symmetry, Bloch's theorem allows us to index the eigenmodes by momentum $\mathbf{k}$ and band index m, i.e. $\psi_{(\mathbf{k},m)}(\mathbf{x}, s) = \varphi_m(\mathbf{k}, s)e^{i\mathbf{k}\cdot\mathbf{x}}$. Henceforth, we shall call the set of eigenvalues $j_{k,m}$ the bandstructure of the circuit, and also refer to the nodes as sites. The impedance between two sites $(\mathbf{0}, s)$ and $(\mathbf{x}, s')$ takes the form

$$
Z_{\mathbf{x}}^{ss'} = \sum_{\mathbf{k},m} \frac{|\varphi_m(\mathbf{k}, s) - \varphi_m(\mathbf{k}, s')e^{i\mathbf{k}\cdot\mathbf{x}}|^2}{j_{\mathbf{k},m}},
\tag{4}
$$

which reduces to $\sum_{\mathbf{k},m} 4j_{\mathbf{k},m}^{-1}|\varphi_m(\mathbf{k}, s)|^2 \sin^2\left(\frac{\mathbf{k}\cdot\mathbf{x}}{2}\right)$ for nodes on the same sublattice $s = s'$. The impedance in Eq. (4) between two nodes becomes large if there exists a finite density of nontrivial eigenmodes with small $j_{\mathbf{k},m}$. Such divergences correspond to resonances in RLC circuits, and will be even more pronounced if the relevant eigenmodes are localized at one region, e.g. a boundary of the circuit or a domain wall trajectory. This is the case for TBRs in topolectrical circuits, where there exists a large density of protected boundary modes with $j_{\mathbf{k},m} \approx 0$. A central result of our work will be the construction of such topolectrical circuits with "grounded" RLC networks, with the ground controlling the pinning of the TBR to $j_{\mathbf{k},m} \approx 0$.

Su–Schrieffer–Heeger circuit. The most elementary 2-band topolectrical circuit can be built from a line of capacitors with alternating capacitances of C_1 and C_2 (Fig. 2a), which is characterized by $t := C_1/C_2$. Note that as will be relevant in the following, changing the initial capacitor to the left from $C_1 \rightarrow C_2$ implies $t \rightarrow 1/t$. Identical inductors L connect the junctions between each capacitor to a common isolated grounding plate. For $t < 1$, a topological boundary mode exists and leads to a drastic increase in circuit impedance, i.e., a TBR. Consider one setup of Fig. 2, with the leftmost grounded capacitor of capacitance $C_1 < C_2$, and another setup with $C_{1,2}$ interchanged. To see that the former arrangement supports a localized "midgap" eigenmode (configuration of potentials) that decays exponentially to the right, while the latter does not, notice that a fixed amount of charge Q between any pair of C_1, C_2 capacitors leads to potential differences V_1, V_2 related by $Q = C_1V_1 = C_2V_2$ between their respective plates. For $t < 1$, there will be a larger potential difference between the plates of C_1 than that of C_2. Indeed, when driven by an AC supply, V_1 and V_2 oscillate in anti-phase with relative amplitude $V_2/V_1 = t$, corresponding to the potential configuration $\psi_0(n) \propto (1, 0, -t, 0, t^2, 0, -t^3, 0, \ldots, ((-t)^n, 0))$, where the index n runs through all 2-node unit cells. $\psi_0(n)$ is exponentially localized at the left end, with a decay length of $\xi = \left(\log\frac{C_2}{C_1}\right)^{-1} = -\log t$. Since $\mathbf{V}$ and the source/sink current $\mathbf{I}$ vanish on the even nodes and are proportional to $(-t)^n$ on the odd nodes, it follows that $\psi_0 \equiv \mathbf{V} \propto \mathbf{I}$, i.e., ψ_0 is an eigenmode of J.

In terms of the grounded circuit Laplacian, the system with periodic boundary conditions is described by

$$
\begin{aligned}
J_{SSH}(k_x) = &i\omega\left(C_1 + C_2 - \frac{1}{\omega^2 L}\right)\mathbb{I} \\
&- i\omega\left[(C_1 + C_2\cos k_x)\sigma_x + C_2\sin k_x\sigma_y\right],
\end{aligned}
\tag{5}
$$

which, up to prefactors, is equivalent to the enigmatic Su-Schrieffer-Heeger (SSH) model developed for midgap states in polyacetylene[2]. Here, σ_x and σ_y are the Pauli matrices defined in the basis consisting of a C_1 capacitor and an adjacent C_2 capacitor on its right. The boundary mode $\psi_0(x)$, where the notation x is now highlighting the site instead of the node interpretation n, is the circuit analog of the SSH zero mode consisting of "dimerized" pairs of capacitors with large amounts of charge oscillating between them. It is topologically protected by a 1D winding number (see methods). For $t < 1$, one finds a nonzero topological winding which cannot be deformed into a trivial winding unless the gap, i.e., the spectral gap of the circuit Laplacian, closes.

Since the left end of the circuit by itself always marks the transition to a trivial regime, for $t < 1$ we expect a boundary mode with vanishing spectral value j_0 in the semi-infinite limit. Indeed, as shown in the appendix, $j_0 \sim (-t)^N$, where N denotes the total number of capacitors. This vanishing eigenvalue marks the TBR, which for open boundary conditions and a hypothetically ideal circuit without serial resistance is characterized by a divergent impedance of $Z_{ab}^{SSH} \sim \frac{(t^{d_a} - t^{d_b})^2}{i\tilde{\omega}C_2(-t)^N}$ (Fig. 2b), where $\tilde{\omega}$ denotes the resonant frequency $\tilde{\omega} = 1/\sqrt{L(C_1 + C_2)}$, and d_a, d_b are the unit cell distances of nodes a and b from the leftmost capacitor.

The theoretical prediction described above is rather precisely what we find experimentally. In the setup depicted in Fig. 2a, we can switch between a capacitor ratio of t and $1/t$ depending on whether we fix the switch to node 1 or 2, which affects the boundary condition where the external voltage source is applied. No midgap mode at the external voltage frequency $\tilde{\omega}$ is observed for $t > 1$, but for $t < 1$. For experimental convenience, we have constrained ourselves to measuring the impedance at the pair of nodes at the boundary, and further map out the midgap voltage profile eigenstate $\psi_0(n)$ of the circuit by measuring the voltage difference between neighboring nodes (Fig. 2c, d). $\psi_0(n)$ displays the predicted behavior within negligible error bars. We find the latter to be a robust measurement, along with the predicted impedance profile if we allow for non-uniformity of circuit elements and consider serial circuit resistance in our calculations (see methods).

Graphene circuit. A more targeted TBR response at the boundaries can be achieved in higher-dimensional topolectrical circuits, where the increased admittance density of states (DOS) from an additional dimension makes it possible to spatially isolate the topolectrical resonance. The SSH circuit can be straightforwardly extended to represent a 2D band structure by adding a spatial modulation to the capacitances with inverse wavelength k_y along a new direction, such that a phase transition at $t = 1$ occurs at a certain range of k_y. This can be achieved, for instance, through the parametrization $C_1 = \gamma + 2\beta\cos k_y$, $C_2 = \gamma + 2\alpha\cos k_y$, bringing the grounded Laplacian to the form

$$
\begin{aligned}
J_{ZZ}(k) = &i\omega\left(2(\gamma + \alpha + \beta) - \frac{1}{\omega^2 L}\right)\mathbb{I} \\
&- i\omega\left(\gamma + 2\beta\cos k_y + \left(\gamma + 2\alpha\cos k_y\right)\cos k_x\right)\sigma_x \\
&- i\omega\left(\gamma + 2\alpha\cos k_y\right)\sin k_x\sigma_y.
\end{aligned}
\tag{6}
$$

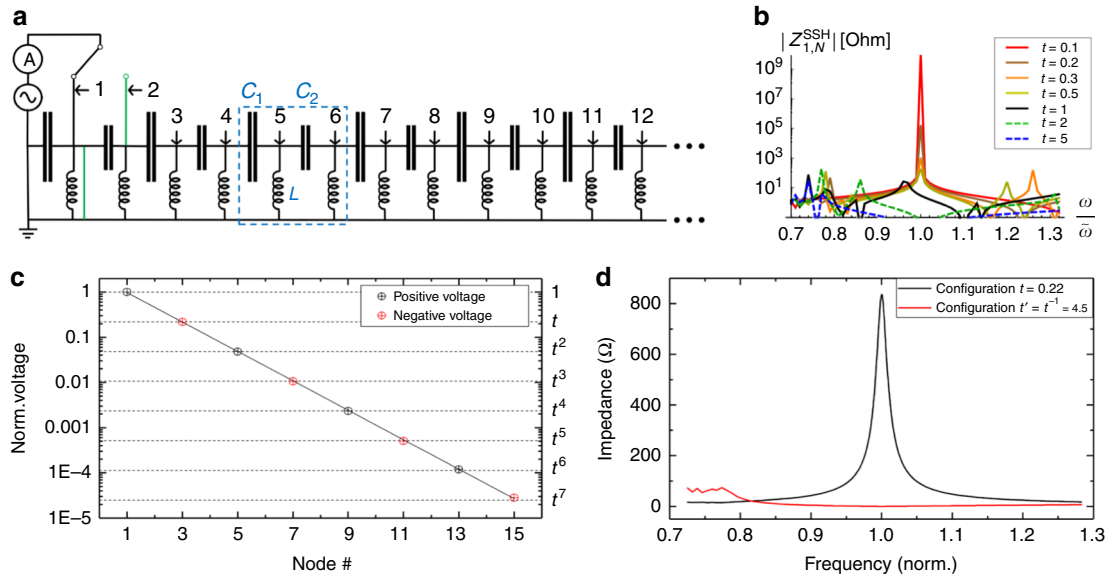In real space, this 2D circuit in Eq. (6) consists of a lattice

Fig. 2 Topolectrical Su-Schrieffer–Heeger (SSH) circuit. **a** circuit diagram blueprint. Each unit cell consists of a pair of capacitors C_1 and C_2, with identical inductors L between every two capacitors. An alternate current (AC) source provides a driving voltage with amplitude V_0. For $t = C_1/C_2 < 1$, an SSH midgap mode is found. In the experimental implementation we set $C_1 = 0.1\,\mu F$, $C_2 = 0.22\,\mu F$ and $L = 10\,\mu H$. Green lines indicate wiring for measuring the t^{-1}-configuration on the same circuit. **b** Ideal impedance magnitude across the nodal ends $a = 1$ and $b = N$ of an $N = 10$ SSH topolectrical circuit as a function of AC frequency ω for various values of t. The dashed curves highlight topologically trivial cases for $t > 1$, showing that the impedance increases enormously only for $t < 1$, the topologically nontrivial regime. The topolectrical boundary resonance (TBR) at $\omega = \tilde\omega$ is most pronounced for the smallest t, and decreases exponentially as t is increased. Secondary resonances are observed at larger deviations from $\tilde\omega$, and are associated with other eigenvalues of the grounded circuit Laplacian J. **c** Measurement of midgap voltage eigenmode $\psi_0(n)$, which accurately fits the shape predicted by theory, i.e., $\psi_0(n) = ((-t)^n V_0, 0)$ for the nth two-site unit cell from the left, see also **a** for node numbering. Associated errors are calculated from standard deviation and according linear regression analysis, but are smaller than the symbols. **d** Impedance measurement of the $t = 0.22$ and $t^{-1} = 4.5$ configuration. Despite non-negligible serial resistance and element non-uniformities, the SSH midgap peak is observed in the impedance measurement but absent for the $t^{-1} = 4.5$ configuration

network with two inequivalent nodes per unit cell, where unlike nodes are connected by capacitors of capacitances α, β, or γ depending on their relative orientations (Fig. 3a). Each node is also connected to the ground by an inductor L. The two-site unit cell, along with the lattice connectivity and edge termination, provides a circuit analog of the zig-zag (ZZ) edge of graphene[18]. This circuit network supports topological boundary modes inherited from its SSH predecessor. If we ground the capacitors on one/both of its edges perpendicular to the x-direction, but leave the circuit periodic along the y-direction by connecting the last capacitor with the first capacitor, a line of singly/doubly degenerate edge modes appear for k_y satisfying $t < 1$, i.e. $(\alpha - \beta)\cos k_y > 0$ (Fig. 3b).

When the AC frequency ω is tuned to the particular resonant frequency $\tilde\omega = \frac{1}{\sqrt{2L(\alpha+\beta+\gamma)}}$, these edge modes correspond to an extensive line of vanishing eigenvalues j_0 that dramatically enhance the circuit impedance at the edge. This can be physically explained in terms of edge resonances involving isolated triplets of simultaneously "dimerized" capacitors sharing oscillating charges, reminiscent of those in the SSH topolectrical circuit. When $\alpha > \beta$ and $|k_y| < \pi/2$, the capacitors in horizontally adjacent unit cells collectively "dimerize" by harboring strongly oscillating charges. Reversing the former condition to $\alpha < \beta$ makes the dimerization incompatible with the edge grounding, while breaking the condition $|k_y| < \pi/2$ also inhibits these oscillations by reversing the relative polarity of adjacent capacitors. Since this dimerization ultimately relies on sublattice symmetry, the TBR only appears when the edges respect sublattice symmetry, such as in the zig-zag case. A realistic implementation is illustrated in Fig. 3, where a serial resistance is attached to each grounding

wire. $Z^{ss'}_{\mathbf{x}_1,\mathbf{x}_2}$ denotes the impedance between the sth node of unit cell $\mathbf{x}_1 = (x_1, y_1)$ and the s'th node of unit cell $\mathbf{x}_2 = (x_2, y_2)$, $s, s' \in \{A, B\}$, the left edge being located at $x = 0$ (see methods). Topologically, the circuit is a cylinder periodic in y-direction, with a circumference of L_y rows. As plotted in Fig. 3c, d for A-type nodes, the impedances in both x and y directions ($Z^{AA}_{(x_1,0),(x_2,0)}$ and $Z^{AA}_{(x,0),(x,y)}$) are greatly enhanced only near the edge, in contrast to the SSH circuit. This enhancement is apparent even for short intervals, as reflected by the rapid rise of impedance $Z^{AA}_{(x,0),(x,y)}$ at small y. For circuits representing higher dimensional band structures, a deeper consequence of Eq. (4) is that the TBR depends on the scale set by the maximal imaginary gap[19], even if the boundary modes themselves are gapless and algebraically decaying.

Weyl circuit. The zig-zag topolectrical circuit, which contains a line of zero eigenvalues when driven at resonant frequency, can be obtained as a slice of a parent 3D lattice of RLC elements with "Fermi arcs" in its bandstructure. One example is the Weyl circuit given, at resonance (see methods), by

$$
\begin{aligned}
J_{\text{Weyl}}(\mathbf{k})\big|_{\omega=\tilde\omega} =\ & -i\tilde\omega\Big(\gamma + 2\beta\cos k_y + \big(\gamma + 2\alpha\cos k_y\big)\cos k_x\Big)\sigma_x \\
& -i\tilde\omega\big(\gamma + 2\alpha\cos k_y\big)\sin k_x\,\sigma_y \\
& +2i\tilde\omega\gamma_z(1 - \cos k_z - \lambda)\sigma_z,
\end{aligned}
\tag{7}
$$

with capacitances, inductances, and resonant frequency satisfying $\tilde\omega^{-2} = 2L(\alpha + \beta + \gamma) = L_z\gamma_z$. This circuit consists of layers of the zig-zag topolectrical circuit connected by capacitors (inductors)
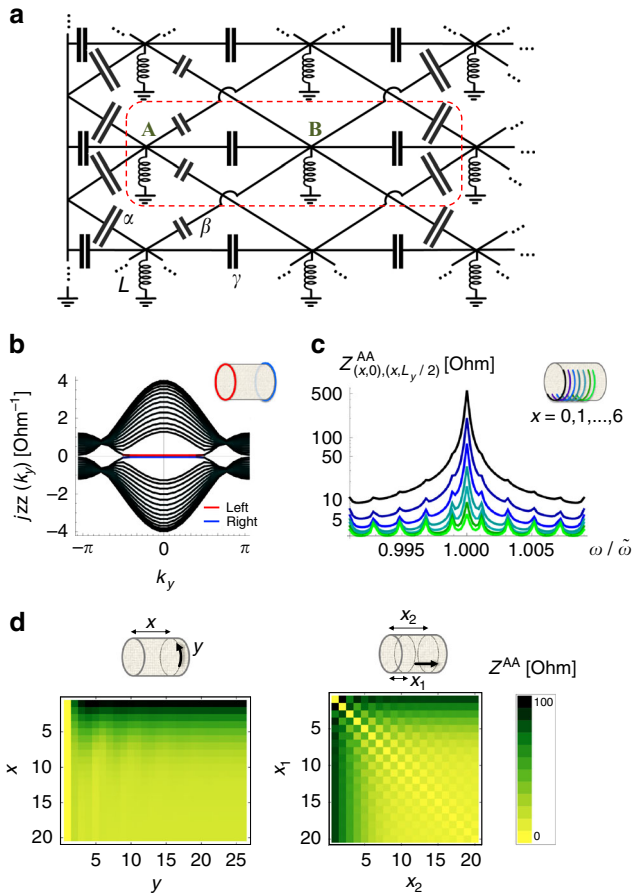
Fig. 3 Topolectrical graphene circuit with a zig-zag edge. **a** circuit diagram. Three types of capacitors connect the nodes in three different orientations, resulting in a two-site unit cell with sublattices denoted by A and B. The circuit is periodically connected in the y-direction with circumference L_y, and grounded on its left and right edges. **b** Admittance bandstructure $j_{zz}(k_y)$ at the resonant AC frequency $\tilde{\omega} = 10^3 s^{-1}$, $L_y = 12$, and capacitor parameters $(\alpha, \beta, \gamma) = (0.8, 0.2, 1)$ mF. At both edges (red/blue), lines of degenerate modes with $j_{0,k_y} \approx 0$ span across the extensive range $|k_y| < \pi/2$. This leads to the TBR depicted in **c**, which displays the impedance $Z^{AA}_{(x,0),(x,L_y/2)}$ between diametrically opposite nodes x sites from the left edge (x = 0). **d** Impedances $Z^{AA}_{(x_1,0),(x_2,0)}$ and $Z^{AA}_{(x,0),(x,y)}$ across intervals perpendicular and parallel to the edges. Note the rapid rise in impedance close to the edge
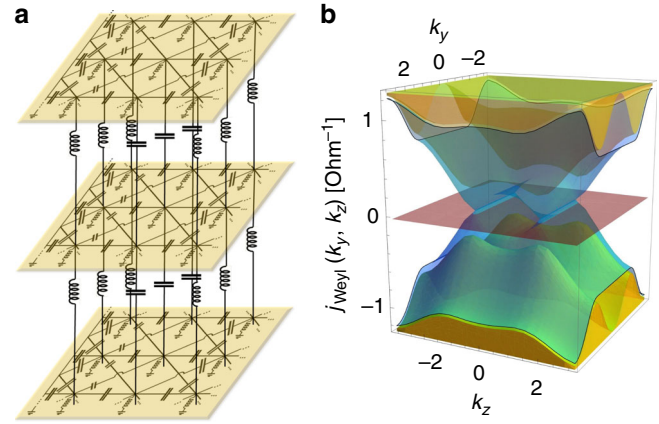

Fig. 4 Topolectrical Weyl circuit. **a** circuit diagram of the Weyl semimetal topolectrical circuit (Eq. (7)). Upon appropriate termination in x-direction, it features resonant bands of modes analogous to Weyl semimetals, as depicted in **b** for parameters $\beta = 0$, $\gamma = 1$, $\alpha = \gamma_z = \lambda = 1/2$. The Weyl circuit is grounded along the plane normal to the x-axis, just as in Fig. 3. Its surface states (blue) separate from the bulk states (yellow), and intersect the $j_{\text{Weyl}}(k_y, k_z) = 0$ plane (brown) along two straight Fermi arcs from $(k_y, k_z) = (-\pi/2, \pm\pi/3)$ to $(\pi/2, \pm\pi/3)$

of strengths $\gamma_z(L_z)$ above A (B) sublattice sites (Fig. 4a). The A (B) site is additionally grounded by an inductor (capacitor) of strength $\frac{1}{2}\lambda^{-1}L_z$ ($2\lambda\gamma_z$). This circuit gives rise to TBRs that bear close similarity to Fermi arcs at zero Fermi energy as found in Weyl semimetals (Fig. 4b). $J_{\text{Weyl}}(k)\big|_{\omega=\tilde{\omega}}$ exhibits four Weyl points at k = $(\pi, \pm\pi/2, \cos^{-1}(1-\lambda))$, which are connected by "Fermi arcs" along both branches of $(\pi, k_y, \cos^{-1}(1-\lambda))$, $|k_y| < \pi/2$ (Fig. 4b). Along these Fermi arcs, we recover the line nodes of the zig-zag topolectrical circuit, where the massive degeneracy is protected by sublattice symmetry.

Discussion

Topolectrical circuits can be realized using basic laboratory equipment. For a realistic implementation, however, as we have

also seen for our experimental implementation of the SSH circuit, one has to take into account the non-uniformity of RLC components, as well as capacitive and resistive losses. We find that disordered topolectrical circuits, which are analogous to topological semimetals, are markly superior to e.g. topological insulator circuits in this respect, as shown in Fig. 5. There, we compare the impedance read-out of our topolectrical circuits containing extensive mode degeneracy (Eqs. (6) and (7)) with that of a topological insulator circuit[9, 20], which we adjusted by grounding it with inductors such that both systems can be accurately tuned for possible TBRs through the AC frequency (see methods). Due to the extensively large boundary DOS which is broadened but not destroyed by disorder (Fig. 6), sharply defined TBRs exist e.g. in the Weyl or zig-zag circuit, even with 10% error tolerance in each circuit element. Furthermore, due to extensivity, the resonances remain pronounced even when disorder shifts them slightly away from $\tilde{\omega}$, i.e., the resonant frequency at zero disorder. By contrast, the impedance resonance peaks of the topological insulator circuit are neither as pronounced nor immune to disorder, since they are mostly due to the bulk modes. Although their boundary modes are likewise topologically protected, they exist at isolated momenta at any given frequency, and thus have limited contribution to the impedance read-out. We find, however, that the voltage eigenstate profile $\psi_0(n)$, as we have measured it for the SSH midgap mode, is still accessible, which we thus propose to be one of the most sensible quantities to measure for topological insulator circuits.

From a broader point of view on 3D topolectrical circuits, the requisite Fermi arcs for TBRs can occur in the presence of more exotic symmetries, e.g., certain non-symmorphic symmetries appearing in known Weyl semimetals or photonic crystals[21]. Many of these symmetries, and hence their accompanying topological phases, can be conveniently realized and designed in electrical circuits, whose network structure is free from physical limitations imposed by the shape of ionic orbitals. Topolectrical circuits are likewise not restricted by intrinsic lengths scales from quantum mechanics, and can be constructed at macroscopic sizes with connections across
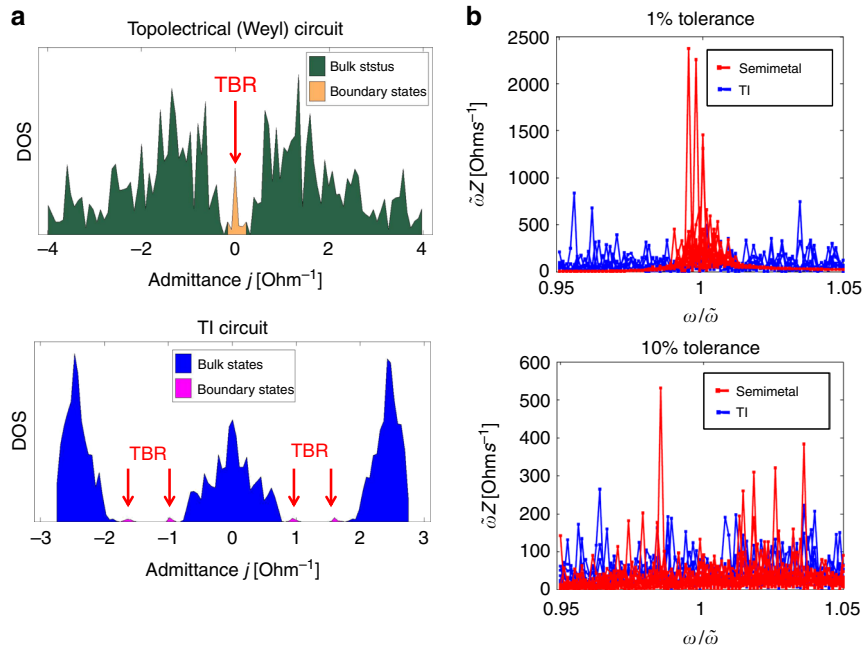
Fig. 5 Disordered topolectrical circuits. **a** Comparison of the DOS of our semimetal topolectrical Weyl circuit with the grounded topological insulator (TI) circuit (see methods), both with component nonuniformity tolerances of 1%. There are extensively more degenerate boundary modes contributing to the TBRs in the semimetal circuit, as compared to the dispersive TI edge modes traversing its three bands. **b** Impedance read-outs of a random ensemble of ten circuits of each type. Each capacitor C/inductor L is further ascribed a resistive loss of $0.1 \times \Delta \left| (i\tilde{\omega}C)^{-1} \right|$ and $0.1 \times \Delta |i\tilde{\omega}L|$, where $\Delta C/C$ ($\Delta L/L$) are 1 or 10%. The semimetal exhibits TBRs that are reasonably robust against disorder. This does not hold for the topological insulator circuit, whose resonances are mainly due to non-universal bulk modes

arbitrarily distant nodes. In particular, topolectrical circuits can be used to simulate higher-dimensional topological phases without involving synthetic dimensions, since each node can be connected to other nodes along more than three axes (Fig. 6). Note, however, that this still poses challenges in terms of multi-layer circuitry design, where the wiring of a multi-layer circuit board, similar to that of highly integrated circuits in general, has to be carefully matched with the given lattice connectivity. The ability to go beyond a regular periodic structure also allows for an accessible study of topological phases on aperiodic networks[22] (Fig. 6) or hyperbolic lattices of arbitrary complexity[23, 24]. Circuit elements such as capacitors can also be mechanically manipulated to break time-reversal symmetry, and induce novel non-equilibrium (Floquet) Chern phases[25]. In general, the TBR can also be designed to appear not at the physical boundary of the circuit, but at domain walls along an arbitrary trajectory through the circuit (Fig. 6). For the zig-zag circuit, such a formulation would bear strong similarity to flux lattice domain walls[26]. This domain wall design would certainly be of interest not just for topolectrical circuits, but also for mechanical systems and beyond.

Methods

Impedance formulae for 2-sublattice periodic circuits. It is instructive to explicitly evaluate Eq. (4) for general 2-node unit cell circuits for periodic boundary conditions (i.e. without grounded terminations). We start from

$$Z_{\mathbf{x}}^{s,s'} = \sum_{\mathbf{k},m} \frac{\left| \varphi_m(\mathbf{k},s) - \varphi_m(\mathbf{k},s')e^{i\mathbf{k}\cdot\mathbf{x}} \right|^2}{j_{\mathbf{k},m}}, \tag{8}$$

where $\mathbf{k}$ denotes momentum, and φ_m are the eigenvectors of $J(\mathbf{k}) = d_0(\mathbf{k}) + \mathbf{d}(\mathbf{k}) \cdot \sigma$, with σ being the vector of Pauli matrices. In closed form, the impedances between

nodes of sublattices A, B separated by $\mathbf{x}$ unit cells are given by (with $\hat{\mathbf{d}} = \mathbf{d}/|\mathbf{d}|$)

$$Z_{\mathbf{x}}^{AA} = \sum_{\mathbf{k},\pm} \frac{1 \pm \hat{d}_3}{d_0 \pm |d|}(1 - \cos \mathbf{k} \cdot \mathbf{x}), \tag{9}$$

$$Z_{\mathbf{x}}^{BB} = \sum_{\mathbf{k},\pm} \frac{1 \mp \hat{d}_3}{d_0 \pm |d|}(1 - \cos \mathbf{k} \cdot \mathbf{x}), \tag{10}$$

$$Z_{\mathbf{x}}^{AB} = \sum_{\mathbf{k},\pm} \frac{1 \pm \sqrt{1 - \hat{d}_3^2}\cos\left(\mathbf{k} \cdot \mathbf{x} + \tan^{-1}\frac{d_2}{d_1}\right)}{d_0 \pm |d|}, \tag{11}$$

$$Z_{\mathbf{x}}^{BA} = \sum_{\mathbf{k},\pm} \frac{1 \pm \sqrt{1 - \hat{d}_3^2}\cos\left(\mathbf{k} \cdot \mathbf{x} - \tan^{-1}\frac{d_2}{d_1}\right)}{d_0 \pm |d|}. \tag{12}$$

Circuit Green's function. A physical interpretation of $G = J^{-1}$ as the inverse of a graph Laplacian is readily obtained. Write $J = D + W - C$, where $[D]_{ab} = \delta_{ab}\sum_c C_{ac}$ is the diagonal matrix of the conductances emanating from each node towards other nodes, $[W]_{ab} = \delta_{ab}w_a$ the conductance of each node towards the ground, and C the adjacency matrix of the conductances. Then

$$G = \frac{1}{D + W - C} = (D + W)^{-1}\sum_{n=0}^{\infty}\left((D + W)^{-1}C\right)^n \tag{13}$$

i.e., G_{ab} is the number of paths of any length from node a to b, each weighted by the conductance ratio (i.e. transition probability) $[(D + W)^{-1}C]_{kl} = C_{kl}/\left(w_k + \sum_{l'}C_{kl'}\right)$ between each pair of nodes k, l along the path. In other words, G keeps track of the fraction of the current that will flow between two nodes, assuming that it spreads out at each node it passes by.

SSH circuit. The simplest topolectrical circuit can be written out in explicit but still compact detail. From Kirchhoff's law, we can write the grounded Laplacian
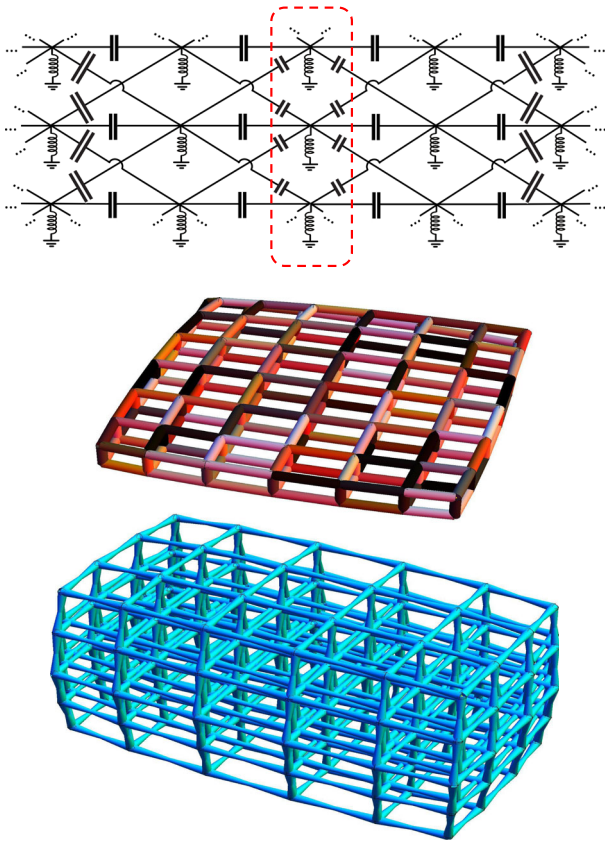
Fig. 6 Generalized topolectrical circuits. To only illustrate a few, topolectrical circuits beyond low-dimensional homogeneous lattice realizations include domain wall states (highlighted by the dashed red rectangle), circuits with aperiodically modulated elements simulating topological quasicrystals (shown in varying tones of red), and circuits on hyperlattices (shown here in blue with 6 × 4 × 4 × 3 unit cells) hosting higher-dimensional states

as

$$J_{SSH} =$$

$$\begin{pmatrix} i\omega(C_1+C_2)+\frac{1}{i\omega L} & -i\omega C_1 & 0 & 0 & 0 & \cdots \\ -i\omega C_1 & i\omega(C_1+C_2)+\frac{1}{i\omega L} & -i\omega C_2 & 0 & 0 & \cdots \\ 0 & -i\omega C_2 & i\omega(C_1+C_2)+\frac{1}{i\omega L} & -i\omega C_1 & 0 & \cdots \\ 0 & 0 & -i\omega C_1 & i\omega(C_1+C_2)+\frac{1}{i\omega L} & -i\omega C_2 & \cdots \\ 0 & 0 & 0 & -i\omega C_2 & i\omega(C_1+C_2)+\frac{1}{i\omega L} & \cdots \\ \vdots & \vdots & \vdots & \vdots & \vdots & \ddots \end{pmatrix}$$

$$= i\omega C_2 \begin{pmatrix} (1+t)(1-\frac{\tilde{\omega}^2}{\omega^2}) & -t & 0 & 0 & 0 & \cdots \\ -t & (1+t)(1-\frac{\tilde{\omega}^2}{\omega^2}) & -1 & 0 & 0 & \cdots \\ 0 & -1 & (1+t)(1-\frac{\tilde{\omega}^2}{\omega^2}) & -t & 0 & \cdots \\ 0 & 0 & -t & (1+t)(1-\frac{\tilde{\omega}^2}{\omega^2}) & -1 & \cdots \\ 0 & 0 & 0 & -1 & (1+t)(1-\frac{\tilde{\omega}^2}{\omega^2}) & \cdots \\ \vdots & \vdots & \vdots & \vdots & \vdots & \ddots \end{pmatrix}.$$

$$(14)$$

with the last diagonal entry containing C_1, C_2 or both depending on which type of capacitor (or both) is connected to the rightmost node. When ω is set to the resonant frequency $\tilde{\omega} = \frac{1}{\sqrt{L(C_1+C_2)}}$, the diagonal terms proportional to the identity disappear, and J possesses an exact expression for its inverse which is

given by

$$G = \frac{1}{i\omega(-t)^n C_2} \begin{pmatrix} 1 & (-t)^{n-1} & -t & (-t)^{n-2} & (-t)^2 & (-t)^{n-3} & \cdots \\ (-t)^{n-1} & 0 & 0 & 0 & 0 & 0 & \cdots \\ -t & 0 & (-t)^2 & (-t)^{n-1} & (-t)^3 & (-t)^{n-2} & \cdots \\ (-t)^{n-2} & 0 & (-t)^{n-1} & 0 & 0 & 0 & \cdots \\ (-t)^2 & 0 & (-t)^3 & 0 & (-t)^4 & (-t)^{n-1} & \cdots \\ (-t)^{n-3} & 0 & (-t)^{n-2} & 0 & (-t)^{n-1} & 0 & \cdots \\ \vdots & \vdots & \vdots & \vdots & \vdots & \vdots & \ddots \end{pmatrix}.$$

$$(15)$$

For $C_1/C_2 = t < 1$, there exists a boundary mode near $(1+t)\left(1-\frac{\tilde{\omega}^2}{\omega^2}\right)$, the middle of the bulk spectral gap of J_{SSH}. Its eigenvalue j_0 can be obtained from the characteristic polynomial of J_{SSH}. At resonant frequency $\omega = \tilde{\omega}$, j_0 is very close to zero, and we can neglect all but the linear term of the characteristic polynomial to obtain

$$j_0 \approx i\tilde{\omega} \frac{(-t)^N (1-t^2)}{1-t^{2\lfloor N/2 \rfloor}}, \tag{16}$$

which exponentially decays with N, the number of capacitors in the SSH circuit. From Eq. (3) and $\psi_0 \propto (1, 0, -t, 0, t^2, \ldots)$, the impedance between nodes 1 and $2x-1$ (or $2x$) is thus given by

$$Z_{1,2x-1}^{SSH} = \frac{|\psi_0(1)-\psi_0(2x-1)|^2}{j_0} = \frac{1}{i\tilde{\omega}C_2} \frac{(1-(-t)^{x-1})^2}{(-t)^N}, \tag{17}$$

$$Z_{1,2x}^{SSH} = \frac{|\psi_0(1)-\psi_0(2x)|^2}{j_0} = \frac{1}{i\tilde{\omega}C_2}\left((-t)^{-N} - 2(-t)^{-x}\right), \tag{18}$$

both of which are plotted in Fig. 2. Note that had C_2 been instead greater than C_1, $\psi_0(x)$ will not be have been able to exist as an eigenmode due to incompatible boundary conditions. However, if the right end of the circuit is also connected to a grounded capacitor C_2, there can be another mirror-reflected, but otherwise identical, boundary mode localized on the right end.

To find the momentum space representation of the grounded Laplacian, we impose periodic boundary conditions and Fourier transform Eq. (14) to obtain Eq. (5).

From Eq. (5), it can be shown that for $t < 1$, J possesses gapped translation-invariant eigenmodes with eigenvalues $j_{k_x,\pm} = C_1 + C_2 - \frac{1}{\omega^2 L} \pm \sqrt{C_1^2 + C_2^2 + 2C_1 C_2 \cos k_x}$. As follows from Eq. (16), there is also a midgap boundary mode with the eigenvalue

$$j_0 \approx C_1 + C_2 - \frac{1}{\omega^2 L} + (-t)^N, \tag{19}$$

which is not small when away from resonance. The SSH circuit has the special property that the decay length $\xi = \log \frac{C_2}{C_1}$ of its boundary mode coincides exactly with the imaginary gap[19, 27], which is the imaginary part of k_x necessary for closing the gap:

$$\sqrt{C_1^2 + C_2^2 + 2C_1 C_2 \cos k_x} = 0 \Rightarrow e^{ik_x} = t \text{ or } t^{-1}. \tag{20}$$

In hindsight, the TBR of the SSH circuit has an elementary interpretation: Due to the special potential profile of the boundary mode (Fig. 2), a driving input voltage V_0 and current I_0 is connected to two capacitors and one inductor, all of which are at zero potential (grounded) at the other end. From the special decaying potential profile, the potential towards the far right (call it node b) must have vanishing potential. By Kirchhoff's law, $I_0 = \left(i\tilde{\omega}(C_1+C_2) - \frac{1}{i\tilde{\omega}L}\right)V_0 \to 0$. Hence follows the impedance $Z_{1b} = \frac{V_0-V_b}{I_0} \approx \frac{V_0}{I_0} \to \infty$.

Equation (5) is a map from S^1 to S^1, and is characterized by an integer winding number

$$\begin{aligned} N_{1D} &= \frac{1}{2\pi} \oint \mathbf{A} \cdot dk \\ &= -\frac{i}{2\pi} \oint \varphi^\dagger \nabla \varphi \, dk_x \\ &= \int_{k_x=0}^{k_x=2\pi} d\left[\tan^{-1}\left(\frac{\sin k_x}{C_1/C_2 + \cos k_x}\right)\right] \\ &= \theta(C_2 - C_1). \end{aligned} \tag{21}$$

The second step of Eq. (21) relies on the absence of a σ_z term in $J_{SSH}(k_x)$, which is enforced by the sublattice symmetry of the circuit (every node looks the same up to a left-right reflection). This winding would not be well-defined if, for instance,

different inductors were connected to different nodes. This winding number N_{1D} is related to the Chern number in the following sense. Consider a 2D extension to J_{SSH} (Eq. (5)). The contribution to N_{2D} from a reciprocal space region R is given by

$$
\begin{aligned}
N_{2D} &= \frac{1}{2\pi}\int_R \nabla \times \mathbf{A}\, d^2k \\
&= \frac{1}{2\pi}\oint_{\partial R} \mathbf{A}\cdot dk \\
&= \frac{1}{4\pi}\int_R \mathbf{d}\cdot\left(\partial_x\mathbf{d}\times\partial_y\mathbf{d}\right)d^2k,
\end{aligned}
\tag{22}
$$

where $\nabla \times \mathbf{A}$ is the Berry flux. Now suppose there is sublattice symmetry, i.e. that there is no σ_3 term so that $\mathbf{d}\perp\hat{e}_3$. Then the second line reduces to a line integral along the equator of the Bloch sphere, which is mathematically known as S^1. Consequently, we can define a *one-dimensional* topological invariant of the winding of the mapping from the 1D torus ∂R to the equator $S^1 \to S^1$, as we did above. This invariant needs the protection of sublattice symmetry; upon breaking it by adding a small σ_3 term, the $\mathbf{d}$ vector will not be confined to the equator, and a second homotopy invariant instead of a first homotopy invariant is required.

With series resistance R on the inductor, which is the most relevant serial resistance to consider, we have the impedance of each inductor replaced by $i\omega L \to i\omega L + R$. The grounded Laplacian is hence replaced by

$$
\begin{aligned}
J'_{SSH} = i\omega\Big[&\left(C_1 + C_2 - \frac{1}{\omega^2(L+R/(i\omega))}\right)\mathbb{I} \\
&- (C_1 + C_2\cos k_x)\sigma_x - C_2\sin k_x\sigma_y\Big]
\end{aligned}
\tag{23}
$$

The TBR resonance peak occurs when the magnitude of the identity matrix term is as small as possible, i.e at the minimal value of

$$
\begin{aligned}
Z_{Res}^{-1} &= \left|i\omega(C_1+C_2) + \frac{1}{i\omega L + R}\right| \\
&= \frac{|(1-\omega^2 L(C_1+C_2)) + i\omega R(C_1+C_2)|}{\sqrt{R^2+\omega^2 L^2}} \\
&= \frac{\sqrt{(1-\omega^2 L(C_1+C_2))^2 + \omega^2 R^2(C_1+C_2)^2}}{\sqrt{R^2+\omega^2 L^2}},
\end{aligned}
$$

which occurs at $\omega^2 = \tilde{\omega}^2 = \frac{1}{L(C_1+C_2)}\sqrt{1 + \frac{2(C_1+C_2)R^2}{L}} - \frac{R^2}{L^2} = \frac{1}{L(C_1+C_2)}\left(\sqrt{1+2\alpha}-\alpha\right)\approx\frac{1}{L(C_1+C_2)}\left(1-\frac{1}{8}\alpha^2\right)$ for small $\alpha = \frac{R^2(C_1+C_2)}{L}$, as can be checked via finding the extremum of the above. For a resonance to occur at a nonzero real frequency, we will need $\alpha < 1 + \sqrt{2}\approx 2.41$, while an accessible resonance realistically requires $\alpha < 10^{-3}$ judging from our simulations. For $R = 28$ mOhm, $L = 10^{-5}$H and $C_1 + C_2 = 1.22\times10^{-7}$F as given in our experimental setup, we have $\alpha \approx 10^{-5}$, which is sufficiently small for a clean and visible resonance. Circuit element non-uniformities hardly have any detrimental effect on the SSH signal, as we checked up to 20% tolerance.

For the experimental implementation of the SSH circuit, a printed circuit board hosting ten unit cells was designed and fit with low serial resistance ($<26m\Omega$) inductors (Coilcraft MA5172-AE) and surface mount multi-layer ceramic chip capacitors (Kemet 0805/1206), respectively. The circuit was fed by an arbitrary waveform generator (Agilent 33220A), the signals were picked up by lock-in amplifier (Zurich Instruments MFLI series).

Zig-zag graphene circuit. The analysis of the zig-zag topolectrical circuit is understood from the viewpoint of employing individual SSH circuits as building blocks (Fig. 3). In real space, the edge mode consists of a superposition of various momenta k_y, each having the decay length of $\xi = (-\log t)^{-1}$, where $t = \frac{\gamma+2\beta\cos k_y}{\gamma+2\alpha\cos k_y}$. The profile of the real space mode is dominated by the slowest decaying k_y mode, and decays algebraically whenever $t = 1$ for some k_y. In our case, this occurs at $\cos k_y = 0$, or everywhere if $\alpha = \beta$. It now may appear that the capacitors of type γ do not affect the qualitative decay of the edge modes. They, however, certainly affect the decay rate of the subdominant contributions, where $\cos k_y \neq 0$. Furthermore, they also affect the Laplacian bulk spectral gap which is given by $4i\omega\min(|\alpha-\beta|, |\alpha-\gamma+\beta|)$, and hence affect the signal to noise ratio of the TBR.

The strength of the TBR depends on the length scale set by the "largest" imaginary gap, which here coincides with $-\log t$, even when the edge modes decay algebraically. To understand why, note that the TBR depends on the divergence of the impedance contributions from *all* eigenmodes (Eq. (3)), especially the modes with "smallest" $\min(t, t^{-1})$. By contrast, the decay rate depends on the nature of the mode with the "largest" $\min(t, t^{-1})$; if the latter is unity, we have algebraic decay even though the TBR stems from the most strongly gapped momentum.

Weyl circuit. The Weyl circuit consists of layers of the zig-zag topolectrical circuits (Fig. 3) connected by capacitors (inductors) of strengths c_z (L_z) at A (B) sublattice sites (Fig. 4a). Each A (B) site is additionally grounded by an inductor (capacitor)

of strength $\frac{1}{2}\lambda^{-1}L_z$ $(2\lambda\gamma_z)$. Its grounded Laplacian is hence given by

$$
\begin{aligned}
J_{Weyl}(\mathbf{k}) =\ & \\
i\omega\Big(2(\gamma+\alpha+\beta) &- \frac{1}{\omega^2 L} + \left(\gamma_z - \frac{1}{\omega^2 L_z}\right)(1-\cos k_z - \lambda)\Big)\mathbb{I} \\
-i\omega\Big(\gamma+2\beta\cos k_y &+ \left(\gamma + 2\alpha\cos k_y\right)\cos k_x\Big)\sigma_x \\
-i\omega\Big(\gamma+2\alpha\cos k_y\Big)&\sin k_x\sigma_y \\
+i\omega\Big(\gamma_z + \frac{1}{\omega^2 L_z}\Big)&(1-\cos k_z - \lambda)\sigma_z
\end{aligned}
\tag{24}
$$

with the resonant frequency $\tilde{\omega}$ given by $2L(\alpha+\beta+\gamma) = L_z c_z = \tilde{\omega}^{-2}$. Equation (24) reduces to Eq. (7) at resonance.

Disordered topolectrical circuits. To illustrate the significance of the semimetal paradigm in the light of the few existing works on electrical circuit realizations of topological phases, we present a detailed comparative analysis of the impedance read-out of our Weyl and zig-zag circuits with those of refs.[9, 20], which realize a topological insulator phase through arrangements of circuit elements possessing appropriate internal symmetry. For a meaningful comparison, we slightly modified their topological insulator circuit by adding grounded capacitors C to every node, so that the AC driving frequency indeed takes the role of the chemical potential in the topological insulator circuit as well.

In the construction of ref. [20], which generalizes that of ref. [9] to arbitrarily large unit cells, the key idea is to realize a topologically nontrivial Z_2 phase protected by a geometric analog of the electronic antiunitary time-reversal operator. Although any RLC circuit must be time-reversal symmetric, it is possible to achieve a nontrivial Z_2 invariant by stacking together two copies of Hofstadter models with opposite magnetic fluxes, entangled in such a way that there is no need of realizing two spatially separated Chern circuits. By connecting unit cells with internal cyclic permutation symmetry with inductors that implement cyclic permutation operations, the electronic time-reversal operator is mapped to a combination of ordinary, i.e. non-projective, time-reversal operations and cyclic permutations.

In our notation, the simplest topological insulator circuit, which contains 3 capacitors per magnetic unit cell (Eq. (3) of ref. [20]), possesses the effective grounded Laplacian consisting of two copies ($\pm$) of

$$
\begin{aligned}
J_{TI}(k) = i\omega\Big[& L_1\begin{pmatrix} 0 & -1 & -e^{ik_x} \\ -1 & 0 & -1 \\ -e^{-ik_x} & -1 & 0 \end{pmatrix} \\
&+ L_2\begin{pmatrix} -2\cos k_y & 0 & 0 \\ 0 & -2\cos(k_y\pm 2\pi/3) & 0 \\ 0 & 0 & -2\cos(k_y\mp 2\pi/3) \end{pmatrix} \\
&2(L_1+L_2)\left(1-\frac{\tilde{\omega}_{TI}^2}{\omega^2}\right)\mathbb{I}_{3\times3}\Big],
\end{aligned}
\tag{25}
$$

where $\tilde{\omega}_{TI}^2 = \frac{1}{2C(L_1+L_2)}$. Note that, opposite to our semimetal circuits, but in accordance to the convention in ref. [20], the ungrounded elements are the inductors, not capacitors. This duplicity yields no extra complication, as the simple relation $\omega \to \frac{\tilde{\omega}^2}{\omega}$ holds when the capacitors and inductors are interchanged. Equation (25) is a variant of (2 opposite copies of) the 3-band Hofstadter Hamiltonian, with each copy possessing 3 bulk bands connected by topological edge modes. The crux is that although these are bona fide topologically protected modes, they do not necessarily contribute significantly to the RLC resonances because they cross a given eigenvalue only at isolated points in momentum space. According to our semimetal paradigm, TBRs are characterized by boundary modes that are (i) extensively degenerate and (ii) spatially localized, with the former not being satisfied by the TI circuit edge mode(s).

To study the precise implications of the absence of extensive degeneracy in a topolectrical circuit, we consider ensembles of disordered circuits, i.e., circuits consisting of elements with nonuniform capacitances C or inductances L. The non-uniformities are characterized by standard errors with tolerances (standard deviations) of 1 or 10%. Additionally, we have included resistive losses proportional to 10% of the non-uniformities of impedances due to disorder. The results are depicted in Fig. 5a, b. It becomes evident that the extensive, semimetal-like degeneracy of our Weyl circuit protects the RLC resonances much better than the protection from the single mode Kramer's degeneracy in the TI circuit. This observation identically holds for both the Weyl and zig-zag topolectrical circuits.

Laplacian formalism. RLC circuits obey a linear 2nd order ordinary differential equation (ODE), just like a mechanical system with springs, dampers and masses, and hence brings up the natural question what the mechanical system analogs of topolectrical circuits are. Topological mechanical systems have already been intensely studied in recent years, although their responses are not typically characterized by an impedance measurement. In a mechanical system with a single polarization direction (e.g. mechanical graphene[28]), the equation of motion

likewise involves the Laplacian: $Lx = M\ddot{x} = -\omega^2 Mx$, i.e.

$$J\mathbf{x} = (L - \omega^2 M)\mathbf{x}. \tag{26}$$

Since the mass matrix is diagonal, it is almost trivial to turn the above into an eigenvalue equation of LM^{-1}, with eigenvalues being ω^2. Nonzero density of states at certain frequencies ω, which are associated with resonances, are by definition also zero eigenstates of J. Usually, these are the only eigenstates of J studied in mechanical systems, since the resonant modes can be directly probed. In electric circuits, the important difference is that direct measurements via the impedance do not only involve these resonant states. From the definition $Z_{ab} = (V_a - V_b)/I$, the impedance measurement can be thought of as a transport problem with an arbitrarily large external driver/probe. This additional complication requires extra information from J, namely, the contributions from all eigenvalues of J, and not just the zero eigenvalue (Eq. (3)). Due to the different orders of time derivatives (powers of ω) entering the equation of motion of an RLC circuit, there is no direct relation between ω and the eigenvalues of J. This is in contrast to mechanical systems, where the mass is local (M is diagonal) and ω^2 can easily be made the eigenvalue. Still, mechanical and electrical resonances are similar in spirit despite being characterized in seemingly opposite ways. In mechanical systems, resonances are associated with minimal dissipation, where small driving perturbations can sustain large oscillations. The same is true for electrical circuits, despite having ostensibly divergent impedance: one then has large voltage oscillations corresponding to small input/output current. Note that, barring specially constructed examples, mechanic systems generally have the restriction that the polarization directions have to be related to the relative spatial displacement of the sites; in electric circuits at laboratory scales, there is no such constraint. Our zig-zag topolectrical circuits can be conveniently carried over to mechanical systems, i.e. in ref. [29] where its Floquet dynamics was also explored. In particular, the generalization from boundary modes to domain wall modes[26] certainly establishes a direction worth considering in mechanical systems as well. This is less obvious for e.g. the Weyl circuit, as higher dimensional networks cannot be realized easily in a mechanical arrangement of springs.

Data availability. The data that support the plots within this paper and other findings of this study are available from the corresponding author upon reasonable request.

References

1. Burkov, A. A. Topological semimetals. *Nat. Mater.* **15**, 1145–1148 (2016).
2. Su, W. P., Schrieffer, J. R. & Heeger, A. J. Solitons in polyacetylene. *Phys. Rev. Lett.* **42**, 1698 (1979).
3. Klitzing, Kv, Dorda, G. & Pepper, M. New method for high-accuracy determination of the fine-structure constant based on quantized hall resistance. *Phys. Rev. Lett.* **45**, 494–497 (1980).
4. Hasan, M. Z. & Kane, C. L. Colloquium: topological insulators. *Rev. Mod. Phys.* **82**, 3045–3067 (2010).
5. Qi, X.-L. & Zhang, S.-C. Topological insulators and superconductors. *Rev. Mod. Phys.* **83**, 1057–1110 (2011).
6. Haldane, F. D. M. & Raghu, S. Possible realization of directional optical waveguides in photonic crystals with broken time-reversal symmetry. *Phys. Rev. Lett.* **100**, 013904 (2008).
7. Lu, L., Joannopoulos, J. D. & Soljačić, M. Topological photonics. *Nat. Photon* **8**, 821–829 (2014).
8. Kane, C. L. & Lubensky, T. C. Topological boundary modes in isostatic lattices. *Nat. Phys.* **10**, 39–45 (2014).
9. Ningyuan, J., Owens, C., Sommer, A., Schuster, D. & Simon, J. Time-and site-resolved dynamics in a topological circuit. *Phys. Rev. X* **5**, 021031 (2015).
10. Süsstrunk, R. & Huber, S. D. Observation of phononic helical edge states in a mechanical topological insulator. *Science* **349**, 47–50 (2015).
11. Yang, Z. et al. Topological acoustics. *Phys. Rev. Lett.* **114**, 114301 (2015).
12. Goldman, N., Budich, J. C. & Zoller, P. Topological quantum matter with ultracold gases in optical lattices. *Nat. Phys.* **12**, 639–645 (2016).
13. Hu, W. et al. Measurement of a topological edge invariant in a microwave network. *Phys. Rev. X* **5**, 011012 (2015).
14. Berry, M. V. Quantal phase factors accompanying adiabatic changes. *Proc. R. Soc. Lond.* **392**, 45–57 (1984).
15. Wan, X., Turner, A. M., Vishwanath, A. & Savrasov, S. Y. Topological semimetal and fermi-arc surface states in the electronic structure of pyrochlore iridates. *Phys. Rev. B* **83**, 205101 (2011).
16. Čerňanová, V., Brenkuš, J. & Stopjakova, V. Non-symmetric finite networks: The two-point resistance. *J. Electr. Eng.* **65**, 283–288 (2014).
17. Cserti, J., Széchenyi, G. & Dávid, G. Uniform tiling with electrical resistors. *J. Phys. A: Math. Theor.* **44**, 215201 (2011).
18. Nakada, K., Fujita, M., Dresselhaus, G. & Dresselhaus, M. S. Edge state in graphene ribbons: nanometer size effect and edge shape dependence. *Phys. Rev. B* **54**, 17954–17961 (1996).
19. Lee, C. H., Arovas, D. P. & Thomale, R. Band flatness optimization through complex analysis. *Phys. Rev. B* **93**, 155155 (2016).
20. Albert, V. V., Glazman, L. I. & Jiang, L. Topological properties of linear circuit lattices. *Phys. Rev. Lett.* **114**, 173902 (2015).
21. Wang, Z., Alexandradinata, A., Cava, R. J. & Bernevig, B. A. Hourglass fermions. *Nature* **532**, 189–194 (2016).
22. Kraus, Y. E., Lahini, Y., Ringel, Z., Verbin, M. & Zilberberg, O. Topological states and adiabatic pumping in quasicrystals. *Phys. Rev. Lett.* **109**, 106402 (2012).
23. Gu, Y. et al. Holographic duality between $(2 + 1)$-dimensional quantum anomalous hall state and $(3 + 1)$-dimensional topological insulators. *Phys. Rev. B* **94**, 125107 (2016).
24. Lee, C. H. Generalized exact holographic mapping with wavelets. *Phys. Rev. B* **96**, 245103 (2017).
25. Oka, T. & Aoki, H. Photovoltaic hall effect in graphene. *Phys. Rev. B* **79**, 081406 (2009).
26. Sessi, P. et al. Robust spin-polarized midgap states at step edges of topological crystalline insulators. *Science* **354**, 1269–1273 (2016).
27. He, L. & Vanderbilt, D. Exponential decay properties of wannier functions and related quantities. *Phys. Rev. Lett.* **86**, 5341 (2001).
28. Socolar, J. E., Lubensky, T. C. & Kane, C. L. Mechanical graphene. *New J. Phys.* **19**, 025003 (2017).
29. Lee, C. H., Li, G., Jin, G., Liu, Y. & Zhang, X. Topological dynamics of gyroscopic and floquet lattices from newton's laws. *Phys. Rev. B* **97**, 085110 (2018).

Author contributions

C.H.L. and R.T. initiated the project and contributed the theoretical analysis. S.I., C.B., F.B., J.B., L.M., and T.K. performed the experiment on the SSH circuit and provided overall guidance in terms of experimental implementation. C.H.L., T.K., and R.T. contributed to writing the manuscript.

Additional information

Competing Interests: The authors declare no competing interests.

Reprints and permission information is available online at http://npg.nature.com/reprintsandpermissions/

Publisher's note: Springer Nature remains neutral with regard to jurisdictional claims in published maps and institutional affiliations.